Stepwise membrane binding of the C2 domains of the extended synaptotagmins revealed by optical tweezers

Jinghua Ge
Yale University School of Medicine https://orcid.org/0000-0002-5820-1521
Xin Bian
Yale University School of Medicine
Lu Ma
Institute of Physics,Chinese Academy of Sciences
Yiying Cai
Yale University School of Medicine
Yanghui Li
Yale University School of Medicine
Jie Yang
Yale University https://orcid.org/0000-0002-3522-0906
Erdem Karatekin
Yale University https://orcid.org/0000-0002-5934-8728
Pietro De Camilli
Department of Cell Biology, Department of Neuroscience, Kavli Institute for Neurosciences, Howard Hughes Medical Institute, Yale University School of Medicine https://orcid.org/0000-0001-9045-0723
Yongli Zhang (yongli.zhang@yale.edu)
https://orcid.org/0000-0001-7079-7973

Article

Keywords: extended synaptotagmins, polypetides, mebrane binding

Posted Date: May 25th, 2021

DOI: https://doi.org/10.21203/rs.3.rs-523346/v1

Version of Record: A version of this preprint was published at Nature Chemical Biology on December 16th, 2021. See the published version at https://doi.org/10.1038/s41589-021-00914-3.

Stepwise membrane binding of the C2 domains of the extended synaptotagmins revealed by optical tweezers

Jinghua Ge[1,‡], **Xin Bian**[1,2,3,4,5,‡], **Lu Ma**[1,6,7,8,‡], **Yiying Cai**[1,2,3,4,‡], **Yanghui Li**[1,9,‡], **Jie Yang**[1], **Erdem Karatekin**[6,7,10,11], **Pietro De Camilli**[1,2,3,4,12], **and Yongli Zhang**[1,10,*]

[1]Department of Cell Biology, Yale University School of Medicine, New Haven, CT 06510, USA

[2]Department of Neuroscience, Yale University School of Medicine, New Haven, CT 06510, USA

[3]Howard Hughes Medical Institute, Yale University School of Medicine, New Haven, CT 06510, USA

[4]Program in Cellular Neuroscience, Neurodegeneration and Repair, Yale University School of Medicine, New Haven, CT 06510, USA

[5]Present address: State Key Laboratory of Medicinal Chemical Biology, College of Life Sciences, Nankai University, Tianjin 300071, China

[6]Department of Cellular and Molecular Physiology, Yale University School of Medicine, New Haven, CT 06510, USA.

[7]Nanobiology Institute, Yale University, West Haven, CT, 06516, USA.

[8]Present address: Beijing National Laboratory for Condensed Matter Physics and CAS Key Laboratory of Soft Matter Physics, Institute of Physics, Chinese Academy of Sciences, Beijing 100190, China

[9]Present address: College of Optical and Electronic Technology, China Jiliang University, Hangzhou 310018, China

[10]Department of Molecular Biophysics and Biochemistry, Yale University, New Haven, CT 06511, USA.

[11]Université de Paris, SPPIN - Saints-Pères Paris Institute for the Neurosciences, Centre National de la Recherche Scientifique (CNRS), F-75006 Paris, France.

[12]Kavli Institute for Neuroscience, Yale University School of Medicine, New Haven, CT 06510, USA

[ǂ]These authors contributed equally to this work.

*Correspondence: yongli.zhang@yale.edu

Abstract

Extended synaptotagmins (E-Syts) mediate lipid exchange between the endoplasmic reticulum (ER) and the plasma membrane (PM). Anchored on ER, E-Syts bind the PM via an array of C2 domains in a Ca^{2+}- and lipid-dependent manner, drawing the two membranes close to facilitate lipid exchange. How these C2 domains bind the PM and regulate the ER-PM distance have not been well understood. Here, we applied optical tweezers to dissect PM membrane binding by E-Syt1 and E-Syt2. We detected Ca^{2+}- and lipid-dependent membrane binding kinetics of both E-Syts and determined the binding energies and rates of individual C2 domains or pairs. We incorporated these parameters in a theoretical model to recapitulate various properties of E-Syt-mediated membrane contacts observed in vivo, including their equilibrium distances and probabilities. Our methods can be applied to study other proteins containing multiple membrane-binding domains linked by disordered polypeptides.

C2 domains are one of the most abundant membrane binding domains, with more than 200 members encoded by human genomes, and participate in numerous biological processes[1-3]. They show diverse affinities for different phospholipids in either Ca^{2+}-dependent or Ca^{2+}-independent manner. In addition, C2 domains often associate with one another or other protein domains[4,5]. Interestingly, multiple C2 domains are found in a variety of integral membrane proteins, especially those involved in membrane tethering leading to fusion or lipid exchange[3,6-8]. These C2 domains often form an array containing two to six C2 domains connected by disordered polypeptides of varying lengths ranging from 5 up to 200 amino acids (Supplementary Fig. 1). These proteins include the synaptotagmins that participate in regulated exocytosis[3]. They also include other proteins thought to participate in membrane fusion such as otoferlin, myoferlin, and dysferlin[6,9], as well as the extended synaptotagmins (E-Syts) that mediate lipid exchanges between the endoplasmic reticulum (ER) and the plasma membrane (PM) without leading to bilayer fusion[8,10-14]. The biological functions and working mechanisms of many of these proteins have not been well characterized. However, it has been shown that C2 repeats are essential for their functions. In many cases, C2 domains in their cytosolically exposed region recognize and bind distinct lipids in another membrane, drawing the two membranes close in a Ca^{2+}-dependent manner to regulate lipid exchange or membrane fusion. Although many methods are available to study membrane binding of isolated C2 domains or domain pairs[15,16], it remains challenging to quantify the interactions between C2 repeats and membranes and their associated tethering force that pulls the two membranes, partly due to lack of an experimental approach and theory to dissect the force-dependent cooperative C2-membrane and C2-C2 interactions. We recently developed a novel approach based on high-resolution optical tweezers to measure protein-membrane interactions[17]. Here, we used this approach for a comprehensive analysis of the membrane interaction of the cytosolic portion of human E-Syt1 and E-Syt2.

E-Syts are a class of evolutionarily conserved proteins (tricalbins in yeast) that comprise an N-terminal hydrophobic hairpin anchored into the ER membrane, a synaptotagmin-like mitochondrial lipid-binding protein (SMP) domain, and a C-terminal C2 repeat containing five C2 domains in E-Syt1 (designated as C2ABCDE) and three C2 domains in E-Syt2 (C2ABC, Fig. 1a) and E-Syt3[7,8,10] (Supplementary Fig.1). Most likely, the C2CD domain pair of E-Syt1 represents a duplication of its C2AB domain, explaining the difference of three otherwise similar paralogues. These folded C2 domains are connected by disordered polypeptides of variable lengths. Regulated by cytosolic Ca^{2+}, the E-Syts participate in tethering the PM and the ER, where most lipids are synthesized, to mediate lipid exchange. Fluorescence and electron microscopy (EM) of cells transfected with tagged E-Syt1 revealed that this protein, when expressed alone, only sparsely populates ER-PM contacts at resting Ca^{2+} level with an average membrane separation in the range of 22-25 nm, while upon elevation of cytosolic Ca^{2+} it undergoes massive accumulation at these sites (resulting in their expansion) in a C2C- and C2E-dependent manner, with an average membrane separation of ~15 nm[10,18-20]. In contrast, transfected tagged E-Syt2 and E-Syt3 are localized constitutively at membrane contact sites even at a resting Ca^{2+} level, with a membrane separation of ~19 nm for overexpressed E-Syt3. The C2C domains in both E-Syt2 and E-Syt3 are required for inducing membrane contacts.

Despite extensive studies, it remains unclear precisely how the E-Syts bind the PM *in trans*, regulate the ER-PM distance in a Ca^{2+}-dependent manner, and transfer lipids[21-24]. In general, C2 domains bind membranes *via* two conserved motifs: a basic patch and a Ca^{2+}-binding site (Supplementary Fig. 2), both of which favor binding of negatively charged lipids enriched in the inner leaflet of the plasma membrane, such as PS and $PI(4,5)P_2$[25]. The C2A and C2C of E-Syt1

and the C2A of E-Syt2 and E-Syt3 contain the Ca^{2+}-binding motif and bind PM at elevated Ca^{2+} levels. In contrast, the C-terminal C2 domains of all three E-Syts (C2E of E-Syt1 and C2C of E-Syt2 and E-Syt3) bear only the basic patch and bind the PM at resting Ca^{2+} levels. In view of this similarity of their C-terminal C2 domains, it is not clear why E-Syt1 and E-Syt2 or E-Syt3 exhibit different efficiency in forming the ER-PM contact sites[10,18-20]. Intriguingly, E-Syt1 C2B and C2D do not contain any obvious membrane binding motifs. Nevertheless, both C2 domains may directly bind membranes or interacts with the corresponding C2A and C2C partners[5,21] to indirectly affect membrane binding. Their exact functions remain to be tested. Furthermore, quantitative understanding of the different efficiency of the three E-Syts in accumulating at, and inducing, ER-PM membrane contacts is lacking. To address these questions, accurate measurements of membrane binding affinities and kinetics of different C2 domains as a function of force, Ca^{2+} concentration, and lipid composition are required. Membrane bridging by E-Syts occurs against a pulling force that typically attenuates binding and promotes unbinding[17]. In addition, a new theory is needed to dissect the cooperativity between different C2 domains in single E-Syts. These experimental and theoretical requirements impose a great challenge to dissect the role of C2 repeats in membrane binding and tethering.

We extended our single-molecule method[17] to measure the force-dependent binding affinities and kinetics of E-Syt1 and E-Syt2 as a function of Ca^{2+} and lipid concentrations. We developed a theory to dissect the cooperativity between different C2 domains and derive membrane binding parameters corresponding to isolated C2 domains. Using these parameters, we calculated the average tethering force, probabilities, and free energy of different C2 binding states. The derived equilibrium membrane separations and their probabilities match the corresponding measurements *in vivo*.

Results

Stepwise binding and unbinding of C2 domains in E-Syt1 and E-Syt2. As in our previous experimental setup[17], we tethered fragments of the C2 containing regions of E-Syt1 and E-Syt2, i.e., E-Syt1 C2ABCDE or E-Syt2 C2ABC, to a bilayer-coated silica bead at its amino terminus and to a polystyrene bead at its carboxy terminus via a 2,260 bp DNA handle (Fig. 1b). The two micron-sized beads were optically trapped with dual-trap optical tweezers and used to detect the tension and extension of the protein-DNA tether. To mediate the attachment, we added an Avi-tag followed by a flexible polypeptide linker to the amino terminus of the protein fragment and a 12-amino-acid (a.a.) SnoopTag to its carboxyl terminus[26]. The SnoopTag was conjugated to its cognate SnoopCatcher protein to which the DNA handle was crosslinked[27]. To mimic the lipid composition of the inner leaflet of the plasma membrane, the supported bilayer consisted of 85 mol% POPC, 10 mol% DOPS, 5 mol% $PI(4,5)P_2$ and 0.03 mol% biotin-PEG-DSPE unless specified otherwise. Finally, we applied tension to the protein fragment by changing the distance between two optical traps (a process that we will refer to as "pulling") at a speed of 10 nm/s (Fig. 1c) or kept the protein at a constant mean force by holding the distance between the two traps constant (Fig. 2).

We first pulled E-Syt1 C2ABCDE in the presence of 100 μM Ca^{2+} in the solution. The resultant force-extension curve (Fig. 1c, FEC #1) exhibits at least two extension jumps at low force (<12 pN, red and green arrows) and up to five jumps at high force (>12 pN, blue arrows). The low force jumps are membrane-dependent, as they disappeared when the experiment was repeated in

the absence of the membrane (Fig. 1c, FEC #2). Thus, these jumps likely resulted from stepwise unbinding of different C2 domains from the bilayer (Fig. 1d). In contrast, the high force jumps are membrane-independent and represents unfolding of individual C2 domains as was observed before[17]. Not all C2 unfolding events were detected in each pulling round, due to premature detachment of the protein-DNA tether from bead surfaces typically above 35 pN. E-Syt2 C2ABC showed similar membrane unbinding transitions at low force and C2 domain unfolding at high force (Fig. 1c, FEC #3-4; Fig. 1d).

Close inspection indicates that the low force jumps were generally reversible with frequent flickering between high and low extensions, indicating fast unbinding and rebinding transitions of C2 domains (Fig. 1c, inset). To better resolve the C2 transitions, we held a single C2ABCDE at different constant mean forces and measured the tether extension over an extended time (Fig. 2a). Despite their fast transitions, three distinct states were discernable, as were confirmed by three peaks in the probability density distributions of extension (Fig. 2b). Accordingly, the extension trajectories were well fit by three-state hidden Markov modeling (Fig. 2a, red curve in the bottom trace), revealing average extensions (Fig. 2a, green dashed lines) and probabilities of all states and transition rates among them (Fig. 3a).

Next, we derived the C2 binding states associated with the three extension levels. E-Syt1 C2ABCDE contains three well-separated membrane-binding modules: C2AB, C2CD, and C2E (Fig. 1a). Binding of each C2 pair would contribute to a single distinct extension, given the proximity of the two C2 domains in each C2 pair, as was observed for Syt1 C2AB[17] and E-Syt2 C2AB[5,21]. Therefore, sequential membrane binding of all three modules would produce four distinct extension levels, including the maximum extension corresponding to the completely unbound state. We noticed that state 3 had the maximum extension among the three observed states and was stable at higher pulling force till C2 unfolding (Fig. 1c, FEC#1). Thus, state 3 represents the completely unbound state. Based on their extensions relative to state 3, state 1 and state 2 probably are C2CD- and C2E-bound states, respectively (Fig. 1d). In contrast, C2AB exhibited no membrane binding in our assay.

To confirm our state assignment, we pulled isolated E-Syt1 C2AB and C2E domains under otherwise identical experimental conditions. Consistent with our derivation, we did not observe any membrane binding of E-Syt1 C2AB (Supplementary Fig. 3). This result was surprising, given the presence of the Ca^{2+} binding motif in C2A, but consistent with the finding that a C2A mutation abolishing its Ca^{2+} binding barely affects membrane tethering by E-Syt1[4]. As reported previously[4], a main role of the Ca^{2+} binding to the C2A domain may be to release the autoinhibitory interaction of this C2 domain with the SMP domain. Interestingly, we detected weak membrane binding of E-Syt1 C2AB when the DOPS concentration was increased from 10% to 20% (Supplementary Fig. 3). In contrast, we observed membrane binding by E-Syt1 C2E alone (Figs. 2c & 1d). Moreover, the binding exhibited fast kinetics as in E-Syt1 C2ABCDE. Taken together, these results corroborated the C2 binding states derived from our measurements (Fig. 1d).

E-Syt2 C2ABC also shows three-state transitions (Figs. 2d-e), consistent with the presence of two C2 binding modules C2AB and C2C. We previously measured the binding energy and kinetics of the two isolated modules[17]. Comparing the binding kinetics of these isolated modules with those of the linked ones as in E-Syt2, E-Syt2 C2AB binding/unbinding transition was consistently faster than that of E-Syt2 C2C. Based on the comparison, we derived a sequential binding model for E-Syt2 (Fig. 1d). Different from E-Syt1 C2AB, E-Syt2 C2AB showed moderate affinity for the membrane with 10% DOPS.

Energetics and kinetics of membrane binding. We analyzed the extension trajectories at constant forces using a three-state hidden-Markov model[28], yielding the probabilities and transition rates of all three states as a function of force (Fig. 3). The modeling revealed the sequential transition rates (i.e., rates for transitions between states 1 and 2 and between states 2 and 3) orders of magnitude higher than non-sequential transition rates (i.e., rates for the transition between states 1 and 3), which confirms the sequential binding and unbinding models for both C2 repeats (Fig. 1d).

We fit the measured probabilities and transition rates using a force-dependent protein-membrane binding model, yielding unbinding energy and binding and unbinding rates of all C2 modules at zero force (Supplementary Table 1)[17,29]. Note that the unbinding energy of each binding module depends on the actual length of the linker tethering the module to the membrane, because the tethering creates an effective local concentration of the C2 binding module around the membrane in a linker length-dependent manner[17]. Using a Gaussian chain model for the disordered linker, we estimated an effective concentration of 0.10-0.22 M for the different C2 binding modules in both E-Syts, given a linker length range of 40-127 amino acids. To facilitate comparison of the binding energy, we calculated the membrane binding energy corresponding to isolated C2 modules in their standard state by normalizing the effective concentration to 1 M (Supplementary Table 1).

The binding affinities obtained by us corroborate previous qualitative observations[4,10,13,18]. Surprisingly, while the C-terminal C2 domains of E-Syt1 and E-Syt2 (i.e. E-Syt1 C2E and E-Syt2 C2C) are closely related to each other, E-Syt1 C2E has much lower membrane binding affinity (6 ± 1 k_BT, mean ± SEM) than E-Syt2 C2C (13.0 ± 0.7 k_BT). This observation suggests that the membrane binding affinity of C2 domains is likely modulated by subtle differences in their canonical binding motifs and residues in other regions. However, the large difference in the binding affinity explains well the different efficiencies of membrane contact formation mediated by both E-Syts[18], as will be clarified in the forthcoming section.

Effect of Ca^{2+} on membrane binding. To characterize Ca^{2+}-dependent membrane binding by E-Syt1 C2ABCDE and E-Syt2 C2ABC, we developed a flow control system to continuously vary Ca^{2+} concentration in the solution where a single C2 repeat was being pulled. To this end, two buffers containing 500 μM EGTA were prepared, one with 600 μM $CaCl_2$ (Ca^{2+} buffer with ~100 μM free Ca^{2+}) and another without $CaCl_2$ (EGTA buffer). The two buffers were then mixed and flowed into the microfluidic flow cell (Fig. 4a). The total calcium concentration in the flow cell ($[Ca^{2+}]$), which consisted of both free and EGTA-chelated calcium, was determined by the volume velocities of the two buffers (V_1 and V_2) before mixing. To test the concentration change scheme, we added 100 nM rhodamine dye to the Ca^{2+} buffer and detected the concentration of the dye in the flow cell based on its fluorescence intensity measured by widefield fluorescence microscopy[30]. We linearly increased the flow rate of the rhodamine-containing Ca^{2+} buffer from 0 to 12 μL/min and simultaneously decreased the flow rate of the EGTA buffer to keep the total flow rate of the two buffers to be 12 μL/min. The dye concentration linearly increased as expected, which justified our concentration change scheme (Fig. 4b). However, although the observation implied that the total calcium concentration in the flow cell varied linearly as predicted, the corresponding free Ca^{2+} concentration ($[Ca^{2+}]$) responded in a nonlinear manner due to the buffering effect of EGTA (see Methods). Combining with the flow control system, we detected C2 membrane binding transitions at constant force while changing Ca^{2+} concentration either continuously in the presence of a flow or stepwise in the absence of flow. While the former method allowed rapid $[Ca^{2+}]$ change

at the expense of slight extra noise in force and extension measurements, the latter method permitted more accurate single-molecule measurement in the absence of flow after each [Ca^{2+}] change (Fig. 4c).

In the presence of 10 μM Ca^{2+}, E-Syt1 C2ABCDE showed robust three-state transitions (Fig. 4c, top trace) as in the presence of 100 μM Ca^{2+} (Fig. 2a). However, the equilibrium force for C2CD transition was reduced, indicating a decrease in C2CD binding energy. In contrast, the C2E transition barely changed. In the absence of Ca^{2+}, the C2CD transition disappeared, whereas the C2E transition shifted to lower force (~2 pN) but with a slight increase in the extension change (Fig. 4c, second trace). The extension increase is consistent with a longer linker tethering C2E to the membrane (203 a.a.), which is equivalent to a direct transition between unbound state 3 and a C2E-bound but C2CD unbound state 1'. Consequently, the accompanying force decrease does not necessarily indicate a reduced affinity of C2E for the membrane[29]. Supporting this view, we repeated the experiment using E-Syt1 C2E with a short linker (60 a.a.) and found that the equilibrium force increased to ~3.4 pN (Fig. 4c, third trace). We determined the binding energy of both C2CD and C2E as a function of Ca^{2+} concentration (Fig. 4d). Consistent with its Ca^{2+} binding motif (Supplementary Fig. 2), C2CD bound the membrane in a Ca^{2+}-dependent manner: the binding was undetectable in the absence of Ca^{2+}, quickly increased in the range of 0.1-10 μM Ca^{2+}, and reached saturation above 50 μM Ca^{2+}. In contrast, C2E binding was Ca^{2+}-independent, consistent with its lack of the Ca^{2+} binding motif.

Similarly, we measured the membrane binding transition of E-Syt2 C2ABC at constant force in the absence of Ca^{2+} (Fig. 4c, bottom trace). The transition was two-state and mediated only by E-Syt2 C2C. Consistent with our early results, E-Syt2 C2AB and C2C bound membranes in a Ca^{2+}-dependent and Ca^{2+}-independent manner, respectively (Supplementary Table 1).

Effects of negatively charged lipids. Previous work suggests that E-Syt C2 domains bind PM by recognizing negatively charged lipids, especially $PI(4,5)P_2$ and DOPS, in the inner leaflet of PM[4,10,19]. To examine the effect of both lipids on membrane binding by C2 repeats, we first increased the $PI(4,5)P_2$ concentration from 5 mol% to 10 mol% and repeated the binding assays. E-Syt1 C2ABCDE continued to bind and unbind sequentially among three states (Fig. 5a). However, both C2CD and C2E transitions shifted to higher force ranges, indicating their tighter membrane binding (compare to Fig. 2a). Moreover, the C2CD transition had greater force shift than C2E, which nearly separated the two otherwise overlapping transitions into different force ranges (Figs. 5a & 5b). Extensive measurements showed that the rise in $PI(4,5)P_2$ concentration from 5% to 10% significantly increased the affinities of C2CD from 10.4 (±0.9) k_BT to 14.5 (±0.9) k_BT and of C2E from 6 (±1) k_BT to 8.4 (±0.3) k_BT. To test whether the membrane binding requires specific lipids, we omitted $PI(4,5)P_2$ but increased DOPS to 30% to keep the charge density the same. We found that while the C2CD affinity was reduced, C2E binding was completely abolished (Fig. 5c & Supplementary Fig. 4). Therefore, C2E specifically binds $PI(4,5)P_2$, whereas C2CD binds both DOPS and $PI(4,5)P_2$, with a preference for the latter. The critical role of $PI(4,5)P_2$ in membrane binding of both C2 modules is consistent with the dramatic effect of $PI(4,5)P_2$ on membrane contact formation observed in cells[10].

A novel inactive conformation of E-Syt2 C2C. Extended measurements of E-Syt2 C2ABC at constant force revealed a fourth state 3' seen as long gaps between the rapid three-state transitions described above (Supplementary Fig. 5). Besides its long dwell time, the state had the same average extension as the C2C-unbound state 3, indicating a new C2C unbound state. The new state

persisted regardless of both Ca^{2+} and E-Syt2 C2AB. These observations suggest that C2C had two unbound states: one was active for binding membranes within tens of milliseconds under our experimental conditions (the active state), whereas the second state was inactive for membrane binding for a longer period (1-200 s, the inactive state) but could slowly return to the active state. It appears unlikely that the inactive C2C state resulted from an inhibitory association of the C2C membrane binding site with the surrounding linker regions, which would lead to its shorter extension than that of the unbound state. The conformation of the inactive C2C state remains to be explored.

Binding kinetics of the cytosolic E-Syt1 dimer. To examine the role of the SMP domain on E-Syt1 membrane binding, we attached the entire cytosolic E-Syt1 dimer to the supported bilayer and pulled an E-Syt1 monomer via its C-terminus as we did for the fragments containing C2 domains only (Supplementary Fig. 6). FECs indicate that the E-Syt1 monomer bound to and unbound from the membrane in a stepwise manner approximately identical to C2ABCDE. The observation was further confirmed by the Ca^{2+}-dependent three-state C2CD and C2E transitions and Ca^{2+}-independent C2E transition at constant force. These comparisons suggest that the SMP domain showed minimal membrane binding affinity and the two E-Syt1 monomers independently bound to the membrane. Our derivation is consistent with the experimental observations that membrane contacts still form with SMP-truncated E-Syt[10] and SMP alone does not bind membranes in trans[4].

Calculations of trans-membrane binding properties of E-Syts. We developed a theory to calculate the trans-membrane binding properties of E-Syts based on the measured membrane binding parameters of isolated C2 modules (Fig. 6a and Supplementary Table 1). The theory considered several salient features of trans-membrane binding (see Methods): (1) different tethering force associated with trans-membrane binding of different C2 modules; (2) force-dependent entropic energy of the polypeptide linkers; (3) force-dependent binding energy and kinetics of each C2 module; and finally (4) cooperativity between successive binding of C2 modules due to the tethering effect. Because the two E-Syt molecules within a single dimer independently bind the membrane, our calculations were performed for a single E-Syt monomer for simplicity.

We first calculated the binding probabilities of different C2 modules and their associated membrane pulling forces as a function of the distance between two stationary planar membranes. In these calculations, the repulsive force between the two apposed membranes was not considered. E-Syt1 C2E is located 76 nm away from the ER membrane as estimated by the contour length of the protein. However, in the absence of Ca^{2+}, C2E only starts to bind PM at 25.0 nm (with 10% binding probability), reaches 50% binding probability at 21.5 nm, and approximately fully binds to PM at 17.5 nm (Fig. 6b, top panel, blue dashed curve). The tethering force depends on the C2 binding state: the force is zero when no C2 modules bound to the membrane and increases as more C2 modules bind the PM. The state-averaged force due to C2E binding reaches a maximum of 1.7 pN at 18.8 nm membrane separation (Fig. 6b, middle panel, cyan dashed curve). In the presence of 100 μM [Ca^{2+}], C2CD dominates membrane binding at a PM distance less than 25.2 nm (Fig. 6b, top panel, red solid curve). In contrast, binding of C2E alone peaks at ~24 nm with a maximum ~10% probability (blue solid curve). Interestingly, significant C2 binding occurs at a higher membrane separation at 24 nm (with ~50% probability) in the presence of Ca^{2+} than at 21.5 nm in its absence (compare red solid and blue dashed curves). These observations are consistent with the

much higher binding affinity of C2CD than that of C2E in the presence of Ca^{2+}. Correspondingly, a single E-Syt1 monomer generates 5.4 pN maximum average tethering force at 22 nm membrane separation (middle panel, cyan solid curve).

E-Syt2 C2C binds to the PM with 50% probability at 26.7 nm in the absence of Ca^{2+} (Fig. 6c; Fig. 6d, top panel), a greater distance than E-Syt1 C2E. This observation is consistent with the fact that C2C has much higher binding affinity than C2E, yet comparable linker length from the ER membrane (Fig. 1a). Accordingly, E-Syt2 C2C generates a maximum average stretching force of 3.7 pN at 26.2 nm membrane separation (Fig. 6d, middle panel). In the presence of 100 Ca^{2+}, C2C binding remains unchanged, whereas C2AB associates with the PM with 50% probability at 13.2 nm and generates maximum tethering force of 5 pN at 12.2 nm.

When either membrane is free to move as in the cell, the tethering force generated by E-Stys will be counteracted by the repulsive force between the two membranes. The membrane separation reaches an equilibrium as the magnitudes of the two forces equate. The repulsive force or potential between ER and PM has not been measured and may depend on many factors, including remodeling of the cell cortex, proteins embedded on both membranes, the detailed architecture of the membrane contact sites, in addition to direct intermembrane interactions, such as membrane undulation and deformation[31,32]. For simplicity, we modeled the repulsive potential with an exponential function as was previously used to simulate SNARE-mediated membrane fusion[33] (see Methods). With this potential, we calculated the membrane repulsive force and total energy of the tethered membranes (Figs. 6b and 6d, middle and bottom panels). Comparing the repulsive force with the tethering force of E-Syt1, we found that the three E-Syt1 binding states can equilibrate at different membrane separations: 15.8 nm for both C2CD and C2E bound state, 19.5 nm for the C2E only bound state, and >35 nm for the unbound state indicating no membrane contact formation (Fig. 6b, middle panel). The probabilities of these states are determined by the Boltzmann distribution based on their associated free energy (Fig. 6b, bottom panel; Supplementary Table 2). In the absence of Ca^{2+}, the C2E bound state has much higher energy (4.3 k_BT) than the unbound state with a large membrane separation (0 k_BT), implying rare formation of ER-PM contacts. In the presence of 100 μM Ca^{2+}, the C2CD- and C2E-bound state dominates with free energy of -1.5 k_BT, indicating robust membrane contact formation. However, C2E is also essential for membrane contact formation by cooperating with C2CD to stabilize the contact. With C2CD alone, the energy of the corresponding C2 tethered state increases to 3.5 k_BT, suggesting poor membrane contact formation (Supplementary Fig. 7 & Supplementary Table 2). All these calculations regarding the average distances and probabilities of the E-Syt1-mediated membrane contacts and their Ca^{2+}- and C2E-dependence are consistent with previous measurements[4,10,18] (Supplementary Table 2).

Similarly, we calculated the parameters associated with E-Syt2-mediated membrane contacts. Without Ca^{2+}, E-Syt2 C2C stably tethers the PM at 19 nm with a free energy of -2.2 k_BT relative to the unbound state (Fig. 6d & Supplementary Table 2). With Ca^{2+}, E-Syt2 C2AB further binds to PM, reducing the membrane separation to 11.3 nm and slightly increasing the free energy to -0.75 k_BT. The C2AB domain is expected to rapidly bind and unbind from the membrane, because the associated energy barrier is small (Fig. 6d, bottom panel, green arrow), which may facilitate lipid transfer. In the absence of C2C, the energy of the C2AB-bound state increases to 10 k_BT, which essentially abolishes membrane contact formation (Supplementary Fig. 7). These calculated parameters are generally consistent with the corresponding in vivo measurements for E-Syt2 or E-Syt3 (Supplementary Table 2)[18].

Discussion

Numerous proteins couple their membrane binding to mechanical force generation or sensing as a key process for their biological functions[34-36]. In turn, mechanical force affects proteins binding to membranes. It is technically challenging to investigate the interplay between mechanical force and protein-membrane interactions. Here we applied optical tweezers to quantify membrane binding of E-Syt1 and E-Syt2. We detected stepwise membrane binding of individual binding modules at different force and extracted the binding affinities of isolated C2 modules. Surprisingly, despite the strong similarities of the two C-terminal C2 domains of E-Syt1 and E-Syt2, we found that E-Syt1 C2E has much lower membrane affinity than E-Syt2 C2C. This difference explains the different ability of two E-Syts to mediate membrane contacts in a resting state when expressed alone[18], as is confirmed by our theoretical modeling. In addition, C2E requires $PI(4,5)P_2$ for its membrane binding and such requirement cannot be substituted by DOPS. Previous studies had suggested that E-Syt1 C2C interacts with C2E in the absence of Ca^{2+} and that such interaction inhibits C2E membrane binding[4,19] unless cytosolic Ca^{2+} is elevated. Our single-molecule experiments did not provide support for this hypothesis and revealed instead that the lack of E-Syt1-mediated membrane contacts in low Ca^{2+} mainly results from the intrinsically weak affinity of the E-Syt1 C2E domain for the PM membrane. It may be possible that an additional auto-inhibitory interaction may be too weak to be detected by our assay[17].

We also discovered that, unlike E-Syt2 C2AB, the closely related E-Syt1 C2AB barely associates with membranes in a moderate concentration of negatively charged lipids. A main function of the Ca^{2+} binding property of this domain is to release an autoinhibitory interaction with the SMP domain which prevents its lipid transport properties[4]. In contrast, E-Syt1 C2CD tightly bind membranes with a Ca^{2+}-dependence consistent with in vivo imaging results[10]. Finally, we developed a theory to predict salient properties of E-Syt-mediated membrane contacts based on the measured C2 binding parameters. Our predictions match well the corresponding experimental measurements in living cells, indicating that E-Syt-mediated membrane contacts can be quantitatively understood by membrane binding of individual C2 domains and their linear arrangement in E-Syts.

Our theoretical modeling revealed new insights and made new predictions on E-Syt-mediated membrane tethering and lipid exchange. Given a maximum tethering force of ~ 5 pN generated by each E-Syt monomer, we estimated that each E-Syt dimer can produce an average force ~ 10 pN. Compared with the force of 10-50 pN to pull out a single membrane tubule from the plasma membranes[31,37], the average force indicates that a few E-Syt dimers may be sufficient to form membrane contact sites. As the first contact forms, one may expect high cooperativity in the binding of other E-Syts to stabilize or expand the contact. Cooperation may also arise from stable heterodimerization of different E-Syts[10]. Together, the cooperation may lead to sequential binding of C2 domains in different E-Syts and corresponding decrease in the ER-PM distance. In a low Ca^{2+} concentration, E-Syt2 or E-Syt3 may start to tether the PM through their C2C domain at a distance >30 nm, which facilitates E-Syt1 C2E binding at ~24 nm (Fig. 6). Ca^{2+} elevation triggers PM binding of E-Syt1 C2CD followed by binding of E-Syt2 C2AB, further reducing the membrane distance to initiate lipid exchange. Future experiments may test these predictions.

Figure legend

Fig. 1. E-Syt C2 domains bind membranes in a stepwise manner as revealed by optical tweezers. (**a**) ER-anchored E-Syts form a dimer via their SMP domains and bind to the plasma membrane (PM) via their tandem C2 domains, pulling the ER-PM membrane close to facilitate lipid transfer in a Ca^{2+}-dependent manner. The lengths of disordered linkers joining different C2 domains are indicated by their numbers in amino acids. (**b**) Schematics of the experimental setup to pull a single E-Syt1 C2 repeat C2ABCDE. (**c**) Force-extension curves (FECs) obtained by pulling single C2 repeats in the presence or absence of the lipid bilayer. Red and green arrows indicate stepwise C2 unbinding from the membrane, and black arrows denotes unfolding of individual C2 domains. (**c**) Schematics of different C2 binding states for some C2 domains or repeats tested in this study.

Fig. 2. E-Syt C2 domains reversibly and sequentially bind to membranes. (**a, c, d**) Extension-time trajectories at constant mean force F for the C2 repeat E-Syt1 C2ABCDE (a), E-Syt1 C2C (c), or E-Syt2 C2ABC (d). The average extensions of three states (numbered on the left as in Fig. 1d) are marked by green dashed lines. A close-up view of the indicated region in the second trajectory in a is shown in the fourth trajectory. The overlaying red trace represents an idealized state transition derived from hidden-Markov modeling (HMM), as in other extension-time trajectories. (**b, e**) Probability density distributions of the extensions shown in **a** or **d** (symbols) and their best fits with a sum of three Gaussian functions (solid curves), with the individual Gaussian functions shown as dashed curves for the black curves.

Fig. 3. Force-dependent probabilities and transition rates of different C2 binding sates for E-Syt1 C2ABCDE (a) and E-Syt2 C2ABC (b). Experimental measurements and their best model fits (see Methods) are indicated by symbols and lines, respectively. The experiments were conducted with 85 mol% POPC, 10 mol% DOPS, 5 mol% $PI(4,5)P_2$, and 0.03 mol% biotin-PEG-DSPE in the presence of 100 μM Ca^{2+}.

Fig. 4. Membrane binding of E-Sty1 C2CD and E-Syt2 C2AB is Ca^{2+}-dependent, while binding of E-Syt1 C2E and E-Syt2 C2C is Ca^{2+}-independent. (**a**) Schematics of the microfluidic system to change Ca^{2+} concentration when a single C2 repeat was being pulled. (**b**) The measured tracing dye concentration and predicted free Ca^{2+} concentration in the flow cell as the flow rate of the Ca^{2+} channel linearly increased from 0 to 12 μL/min while keeping the total flow rate of the two channels at 12 μL/min. (**c**) Extension-time trajectories at constant force in different Ca^{2+} concentrations. (**d**) Unbinding free energy of E-Syt1 C2CD and C2E as a function $[Ca^{2+}]$.

Fig. 5. Membrane binding of E-Syt1 C2CD and C2E differentially depends upon $PI(4,5)P_2$ and DOPS. (**a**) Extension-time trajectories of E-Syt1 C2ABCDE at constant force with 10 mol% $PI(4,5)P_2$. (**b**) Force-dependent probabilities and transition rates of different E-Syt1 binding states (symbols) and their best model fits (lines). (**c**) Extension-time trajectory of E-Syt1 C2ABCDE at constant force in the presence of 30% DOPS.

Fig. 6. Properties of E-Syt-mediated ER-PM contacts can be theoretically modeled. (**a, c**) Schematics of different C2 binding and membrane tethering states of E-Syt1 (a) or E-Syt2 (c) in the absence and presence of Ca^{2+}. (**b, d**) Calculated probabilities (top panel), tethering force (middle), and total free energy (bottom) of different states of E-Syt1 (b) or E-Syt2 (d). Calculations

corresponding to the presence of Ca^{2+} or the absence of Ca^{2+} are indicated by solid and dashed lines, respectively. Stable and unstable states are indicated by solid and hollow circles, respectively.

Methods

Plasmids and protein constructs. The gene coding for residues 93-1104 (SMP-C2ABCDE), 321-1104 (C2ABCDE) or 936-1104 (C2E) of human E-Syt1 was cloned into the pCMV6-An-His vector. The regions coding for residues 321-603 of human E-Syt1 (C2AB) and residues 343-893 of human E-Syt2 (C2ABC) were cloned into the pET-SUMO vector. In both vectors, an Avi tag was inserted between the His tag and the protein and a SnoopTag just after the protein. The plasmid encoding E-Syt2 C2 was previously described[4,17]. The amino acid sequences of all the protein constructs are shown in Supplementary Information.

Protein constructs, expression, and purification

Expression in eukaryotic cells. E-Syt1 SMP-C2ABCDE, E-Syt1 C2ABCDE, or E-Syt1 C2E was expressed in Expi293 cells with an N-terminal His_6-tag, as described previously[4,13]. Cells were harvested and lysed in buffer A [25 mM Tris-HCl, pH 8.0, 300 mM NaCl, 10 mM imidazole, 1× complete EDTA-free protease inhibitor cocktail (Roche), 0.5 mM TCEP] by three freeze–thawing cycles using liquid nitrogen. The lysates were clarified by centrifugation at 17,000 x g for 30 min, and the protein was purified by a Ni-NTA column (Clontech), and was further purified by gel filtration (Superdex 200, GE Healthcare) in buffer B (25 mM Tris-HCl, pH 8.0, 100 mM NaCl, 0.5 mM TCEP). Fractions containing E-Syt1 were pooled and concentrated to ~1 mg/ml.

Expression in bacteria. E-Syt1 C2AB, E-Syt2 C2ABC, or E-Syt2 C2C was transformed into BL21 (DE3) RIL Codon Plus (Agilent) *E. coli* cells. Cells were grown in Super Broth medium at 37 °C to an OD600 of 0.6, and the expression was induced by addition of 0.5 mM IPTG for 20 h at 18 °C. The cells were harvested and lysed by sonication in buffer A. The lysates were clarified by centrifugation at 30,000 x g for 1 h, and the protein was isolated by a Ni-NTA column, and further purified by gel filtration in buffer B. Fractions containing the target protein were pooled and concentrated to ~1 mg/ml. The proteins with SUMO tag were digested by SUMO protease over night at 4 °C and then were further purified by Ni-NTA column followed by gel filtration in buffer B.

Protein and DNA handle conjugation

A unique cysteine residue was introduced to SnoopCatcher and used to crosslink to the thiol-containing 2,260 bp DNA handle as previously described[38]. The purified E-Syt fragments were biotinylated using BirA biotin ligase (BirA500, Avidity), with free biotin removed by gel filtration (Micro Bio-Spin 6 Columns, Bio-Rad). The E-Syt constructs containing the Snoop tag were mixed with the SnoopCatcher-DNA handle mixture with 5:1 molar ratio of E-Syt protein to SnoopCatcher and then incubated overnight to conjugate the E-Syt proteins to the DNA handles via SnoopCatcher.

Membrane coating on silica beads

The protocol to prepare membrane-coated silica beads has been detailed elsewhere[17]. Briefly, a mixture of chloroform-dissolved lipids was dried under a nitrogen flow followed by evaporation in vacuum for one hour. The dried lipids were then rehydrated in the HEPES buffer containing 25

mM HEPES, pH7.4, and 200 mM NaCl. Small unilamellar vesicles (SUVs) were formed by sonication and centrifugation of the hydrated lipids. The silica beads (2.0 μm, SS04N, Bangs Laboratories) were added to the SUVs and vortexed at 37 °C for 45 minutes. SUVs spontaneously collapsed to the surfaces of the silica beads to form supported bilayers. The beads were then washed five times using the HEPES buffer to remove excessive SUVs through cycles of centrifugation at 10,000 rpm for 45 seconds and resuspension. All lipids were purchased from Avanti Polar Lipids: POPC (850457P), DOPS (840035P), Brain PI(4,5)P_2 (840046X), Biotin-PEG(2000)-DSPE (880129P).

Dual-trap high-resolution optical tweezers

The dual-trap high-resolution optical tweezers are described elsewhere in detail[17,30,39]. The optical tweezers are assembled on an optical table (TMC, MA) located in an acoustically isolated and temperature-controlled room. A 1064 nm laser beam from a solid-state laser (Spectra-Physics, CA) is expanded approximately fivefold by a telescope and split into two orthogonally polarized beams. The beams are reflected by two mirrors: one is fixed and the other is mounted on a high-resolution piezoelectric actuator (Mad City Labs, WI) that turns the mirror in two directions. The two beams are combined, further expanded two-fold by a second telescope, and focused using a water immersion 60X objective with a numerical aperture of 1.2 (Olympus, PA) to form two optical traps around the center of a microfluidic chamber[40]. The outgoing laser beams are collected and collimated by another objective, split by polarization, and projected to two position-sensitive detectors (Pacific Silicon Sensor, CA). The displacements of two trapped beads were detected using back-focal-plane interferometry[41]. An EMCCD camera (Andor iXon3) is used to for wide-field epifluorescence imaging[30]. The tweezers were operated using a computer interface written in LabVIEW (National Instruments, TX).

Flow control system

The two flows to the central flow cell were independently controlled using computer-controlled pressure regulators (MS4-LR, Festo, NY) in combination with flow sensors (SLI-0430, Sensirion, Switzerland) that measure the flow rates. The constant flow rate was achieved by adjusting the pressure in the sample vial through PID feedback control using a LabVIEW interface. Both the Ca^{2+} buffer and the EGTA buffer contained 200 mM NaCl, 25 mM HEPES pH 7.4, and 500 μM EGTA, while the Ca^{2+} buffer additionally contained 600 μM $CaCl_2$. The free Ca^{2+} concentration in the flow cell was calculated using Maxchelator (Web version v1.2) based on the total concentrations of calcium and EGTA.

Single-molecule manipulation experiments

The single molecule experiments have been detailed elsewhere[17,38]. An aliquot of the protein-DNA conjugate mixture was bound to anti-digoxigenin antibody-coated polystyrene beads 2.1 μm in diameter (Spherotech, IL) and injected to the top microfluidic channel, while the membrane-coated silica beads were injected to the bottom channel. Two beads were captured by optical traps and their Brownian motions were measured to determine the stiffnesses of the two traps. The beads were then brought close to form tethers between two bead surfaces. The pulling experiments were performed at room temperature (~23 ºC) in 25 mM HEPES, pH 7.4, 200 mM NaCl, 500 μM EGTA, 0-1 mM $CaCl_2$, and the oxygen-scavenging system[38].

Hidden-Markov modeling (HMM) and derivations of binding energy and kinetics

Methods and algorithms of HMM and energy and rate derivations are detailed elsewhere[28,29,38], including the MATLAB codes used for these calculations[42]. Briefly, extension-time trajectories at constant trap separations were mean-filtered using a time window of 1-3 ms and then analyzed by two- or three-state HMM, which revealed probabilities and average extensions of all states and their associated transition rates. The corresponding idealized state transitions were calculated using the Viterbi algorithm. Methods to derive binding energy and kinetics in the presence and absence of membrane tethers were described elsewhere[17]. Briefly, the free energy of each state was determined based on the Boltzmann distribution, while the binding and unbinding rates were calculated based on the Kramers equation. These parameters at zero force were obtained by simultaneously fitting the measured probabilities and extensions of all states and their transition rates using a nonlinear model[29].

Calculations of trans-membrane binding properties of E-Syts

The average force (F) of each C2 binding state (Figs. 6b & 6d, middle panel) was calculated using the worm-like chain model[43]

$$F = \frac{k_B T}{P}\left[\frac{1}{4\left(1-\frac{x}{L}\right)^2}+\frac{x}{L}-\frac{1}{4}\right], \tag{1}$$

where L and x are the total contour length and extension, respectively, of the stretched polypeptide linkers due to the trans-membrane binding, and P =0.6 nm is the persistence length of the polypeptide[17]. The contour length per amino acid was chosen as 0.365 nm. The extension was equal to the membrane separation (d) subtracted by the total length of folded C2 proteins under tension in the pulling direction (2~6 nm)[29]. The total free energy of the tethered membranes (E_t , Figs. 6b & 6d, bottom panel) was the sum of the entropic energy of the stretched polypeptide linkers ($E_{stretch}$), the total C2-membrane binding energy, and the membrane repulsive energy (V). The entropic energy of the polypeptide was calculated based on the worm-like chain model[29] with

$$E_{stretch} = \frac{k_B T}{P}\frac{L}{4\left(1-\frac{x}{L}\right)}\left[3\left(\frac{x}{L}\right)^2-2\left(\frac{x}{L}\right)^3\right]. \tag{2}$$

To calculate the total C2-membrane binding energy, we distinguished membrane-bound C2 modules that are not loaded by the stretching force (e.g., E-Syt1 C2E in the bound state i in Fig. 6a) and those that are (e.g., E-Syt1 C2CD in the bound state i). The former has the membrane binding energy ($E_b^{(unload)}$) and binding rate (k_b) derived from the measured binding and unbinding rates corresponding to the isolated C2 module (k_{on} , and k_{ub} in Supplementary Table 1) due to the tethering effect, i.e.,

$$k_b = k_{on} c, \quad E_b^{(unload)} = k_b / k_{ub}, \tag{3}$$

where

$$c = \frac{1}{sN_A}\left(\frac{3}{4\pi P l}\right)^{\frac{1}{2}} \tag{4}$$

is the effective concentration of a C2 module around the membrane[17]. Here, the C2 module is tethered to the membrane by a polypeptide linker with a contour length l , $s = 0.7$ nm^2 is the area

per lipid, and N_A =6.02×10^{23} per mole the Avogadro constant. For example, E-Syt1 C2E in the bound state i in Fig. 6a has $l = 25.6$ nm (Fig. 1a). The membrane binding parameters of the force loaded C2 module are modulated by both the tethering effect and the stretching force. The tethering effect was considered in the same way as the force unloaded C2 modules, but with a different contour length of the linker that connects the force loaded module to the ER membrane, which yielded the corresponding membrane binding rate (k_b), and unbinding rate (k_{ub}) in the absence of force. In the presence of the stretching force, the binding rate, the unbinding rate, and the binding energy become

$$k_b^{'} = k_b \exp\left(-\frac{E_{stretch}}{k_B T}\right), \quad k_{ub}^{'} = k_{ub} \exp\left(\frac{F\Delta x}{k_B T}\right), \quad E_b^{(load)} = \frac{k_b^{'}}{k_{ub}^{'}}, \tag{5}$$

respectively, where Δx is the distance between the location of the energy barrier for the binding and unbinding transition state and the location of the energy well for the bound state determined from the pulling experiment[29]. The repulsive energy between the two membranes was chosen as

$$V(d) = E_m \exp\left[-\frac{d - d_c}{d_1}\right], \tag{6}$$

where E_m =35 k_BT, d_c =1 nm, and d_1 =10 nm[33]. Thus, the total energy of the E-Syt-tethered membranes was calculated as

$$E_t = E_{stretch} + E_b^{(unload)} + E_b^{(load)} + V, \tag{7}$$

as shown in Figs. 6b and 6d, bottom panel. Except for $E_b^{(unload)}$, all energy terms here are functions of membrane separation d. In addition, the first three terms are state-dependent. Finally, the state populations were computed based on the Boltzmann distribution (Figs. 6b & 6d, top panel)

Acknowledgements
We thank J. Jiao and A. Rebane for technical assistance. This work was supported by NIH grants R35GM131714, R01GM093341, and R01GM120193 to Y. Z.; R01NS113236 to E.K.; NS36251 and DA018343 to PDC.

Competing interests
The authors declare no competing interests.

Author contributions
All authors designed the experiments and analyzed the data, J. G., L. M., Y. L. performed the single-molecule experiments, J. G., X. B., L. M., Y. C. purified the proteins and DNA, Y. Z. performed the calculations shown in Fig. 6. J. G., X. B., E. K., P. C. D., Y. Z. wrote the paper.

Additional information
Supplementary information is available for this paper.

References

1. Lemmon, M. A. Membrane recognition by phospholipid-binding domains. *Nat Rev Mol Cell Bio* **9**, 99-111 (2008).
2. Hurley, J. H. Membrane binding domains. *Biochim. Biophys. Acta* **1761**, 805-11 (2006).
3. Pinheiro, P. S., Houy, S. & Sorensen, J. B. C2-domain containing calcium sensors in neuroendocrine secretion. *J. Neurochem.* **139**, 943-958 (2016).
4. Bian, X., Saheki, Y. & De Camilli, P. Ca^{2+} releases E-Syt1 autoinhibition to couple ER-plasma membrane tethering with lipid transport. *EMBO J.* **37**, 219-234 (2018).
5. Xu, J. J. et al. Structure and Ca^{2+}-binding properties of the tandem C2 domains of E-Syt2. *Structure* **22**, 269-280 (2014).
6. Pangrsic, T., Reisinger, E. & Moser, T. Otoferlin: a multi-C_2 domain protein essential for hearing. *Trends Neurosci.* **35**, 671-680 (2012).
7. Min, S. W., Chang, W. P. & Sudhof, T. C. E-Syts, a family of membranous Ca^{2+}-sensor proteins with multiple C_2 domains. *PNAS* **104**, 3823-3828 (2007).
8. Saheki, Y. & De Camilli, P. The extended-synaptotagmins. *Biochim. Biophys. Acta* **1864**, 1490-1493 (2017).
9. Lek, A., Evesson, F. J., Sutton, R. B., North, K. N. & Cooper, S. T. Ferlins: regulators of vesicle fusion for auditory neurotransmission, receptor trafficking and membrane repair. *Traffic* **13**, 185-94 (2012).
10. Giordano, F. et al. PI(4,5)P_2-dependent and Ca^{2+}-regulated ER-PM interactions mediated by the extended synaptotagmins. *Cell* **153**, 1494-1509 (2013).
11. Chang, C. L. et al. Feedback regulation of receptor-induced Ca^{2+} signaling mediated by E-Syt1 and Nir2 at endoplasmic reticulum-plasma membrane junctions. *Cell Rep* **5**, 813-825 (2013).
12. Saheki, Y. & De Camilli, P. Endoplasmic reticulum-plasma membrane contact sites. *Annu. Rev. Biochem.* **86**, 659-684 (2017).
13. Saheki, Y. et al. Control of plasma membrane lipid homeostasis by the extended synaptotagmins. *Nat. Cell Biol.* **18**, 504-515 (2016).
14. Yu, H. J. et al. Extended synaptotagmins are Ca^{2+}-dependent lipid transfer proteins at membrane contact sites. *PNAS* **113**, 4362-4367 (2016).
15. Zhao, H. X. & Lappalainen, P. A simple guide to biochemical approaches for analyzing protein-lipid interactions. *Mol Biol Cell* **23**, 2823-2830 (2012).
16. Knight, J. D., Lerner, M. G., Marcano-Velazquez, J. G., Pastor, R. W. & Falke, J. J. Single molecule diffusion of membrane-bound proteins: window into lipid contacts and bilayer dynamics. *Biophys. J.* **99**, 2879-87 (2010).
17. Ma, L. et al. Single-molecule force spectroscopy of protein-membrane interactions. *Elife* **6**, e30493 (2017).
18. Fernandez-Busnadiego, R., Saheki, Y. & De Camilli, P. Three-dimensional architecture of extended synaptotagmin-mediated endoplasmic reticulum-plasma membrane contact sites. *Proc. Natl. Acad. Sci. U.S.A.* **112**, E2004-13 (2015).
19. Idevall-Hagren, O., Lu, A., Xie, B. & De Camilli, P. Triggered Ca^{2+} influx is required for extended synaptotagmin 1-induced ER-plasma membrane tethering. *EMBO J.* **34**, 2291-305 (2015).
20. Kang, F. et al. E-syt1 re-arranges STIM1 clusters to stabilize ring-shaped ER-PM contact sites and accelerate Ca^{2+} store replenishment. *Sci Rep* **9**, 3975 (2019).
21. Schauder, C. M. et al. Structure of a lipid-bound extended synaptotagmin indicates a role in lipid transfer. *Nature* **510**, 552-555 (2014).

22. Bian, X., Zhang, Z., Xiong, Q. C., De Camilli, P. & Lin, C. X. A programmable DNA-origami platform for studying lipid transfer between bilayers. *Nat. Chem. Biol.* **15**, 830-+ (2019).
23. Li, P. Q., Lees, J. A., Lusk, C. P. & Reinisch, K. M. Cryo-EM reconstruction of a VPS13 fragment reveals a long groove to channel lipids between membranes. *J. Cell Biol.* **219**, e202001161 (2020).
24. Wong, L. H., Gatta, A. T. & Levine, T. P. Lipid transfer proteins: the lipid commute via shuttles, bridges and tubes. *Nat Rev Mol Cell Bio* **20**, 85-101 (2019).
25. Corbalan-Garcia, S. & Gomez-Fernandez, J. C. Signaling through C2 domains: More than one lipid target. *Biochimica Et Biophysica Acta-Biomembranes* **1838**, 1536-1547 (2014).
26. Veggiani, G. et al. Programmable polyproteams built using twin peptide superglues. *PNAS* **113**, 1202-1207 (2016).
27. Min, D., Jefferson, R. E., Bowie, J. U. & Yoon, T. Y. Mapping the energy landscape for second-stage folding of a single membrane protein. *Nat. Chem. Biol.* **11**, 981-987 (2015).
28. Zhang, Y. L., Jiao, J. & Rebane, A. A. Hidden Markov modeling with detailed balance and its application to single protein folding *Biophys. J.* **111**, 2110-2124 (2016).
29. Rebane, A. A., Ma, L. & Zhang, Y. L. Structure-based derivation of protein folding intermediates and energies from optical tweezers. *Biophys. J.* **110**, 441-454 (2016).
30. Sirinakis, G., Ren, Y. X., Gao, Y., Xi, Z. Q. & Zhang, Y. L. Combined and versatile high-resolution optical tweezers and single-molecule fluorescence microscopy. *Rev Sci Instrum* **83**, 093708 (2012).
31. Sheetz, M. P. Cell control by membrane-cytoskeleton adhesion. *Nat Rev Mol Cell Bio* **2**, 392-396 (2001).
32. Cowley, A. C., Fuller, N. L., Rand, R. P. & Parsegian, V. A. Measurement of repulsive forces between charged phospholipid bilayers. *Biochemistry-Us* **17**, 3163-3168 (1978).
33. Zorman, S. et al. Common intermediates and kinetics, but different energetics, in the assembly of SNARE proteins. *Elife* **3**, e03348 (2014).
34. Shen, H., Pirruccello, M. & De Camilli, P. SnapShot: membrane curvature sensors and generators. *Cell* **150**, 1300, 1300 e1-2 (2012).
35. Ross, T. D. et al. Integrins in mechanotransduction. *Curr. Opin. Cell Biol.* **25**, 613-618 (2013).
36. Basu, R. et al. Cytotoxic T cells use mechanical force to potentiate target cell killing. *Cell* **165**, 100-110 (2016).
37. Brownell, W. E., Qian, F. & Anvari, B. Cell membrane tethers generate mechanical force in response to electrical stimulation. *Biophys. J.* **99**, 845-852 (2010).
38. Jiao, J. Y., Rebane, A. A., Ma, L. & Zhang, Y. L. Single-molecule protein folding experiments using high-resolution optical tweezers. *Methods Mol Biol* **1486**, 357-390 (2017).
39. Moffitt, J. R., Chemla, Y. R., Izhaky, D. & Bustamante, C. Differential detection of dual traps improves the spatial resolution of optical tweezers. *PNAS* **103**, 9006-9011 (2006).
40. Zhang, Y. L., Sirinakis, G., Gundersen, G., Xi, Z. Q. & Gao, Y. DNA translocation of ATP-dependent chromatin remodelling factors revealed by high-resolution optical tweezers. *Methods Enzymol.* **513**, 3-28 (2012).
41. Gittes, F. & Schmidt, C. F. Interference model for back-focal-plane displacement detection in optical tweezers. *Optics Letters* **23**, 7-9 (1998).

42. Gao, Y. et al. Single reconstituted neuronal SNARE complexes zipper in three distinct stages. *Science* **337**, 1340-1343 (2012).
43. Marko, J. F. & Siggia, E. D. Stretching DNA. *Macromolecules* **28**, 8759-8770 (1995).

Figures

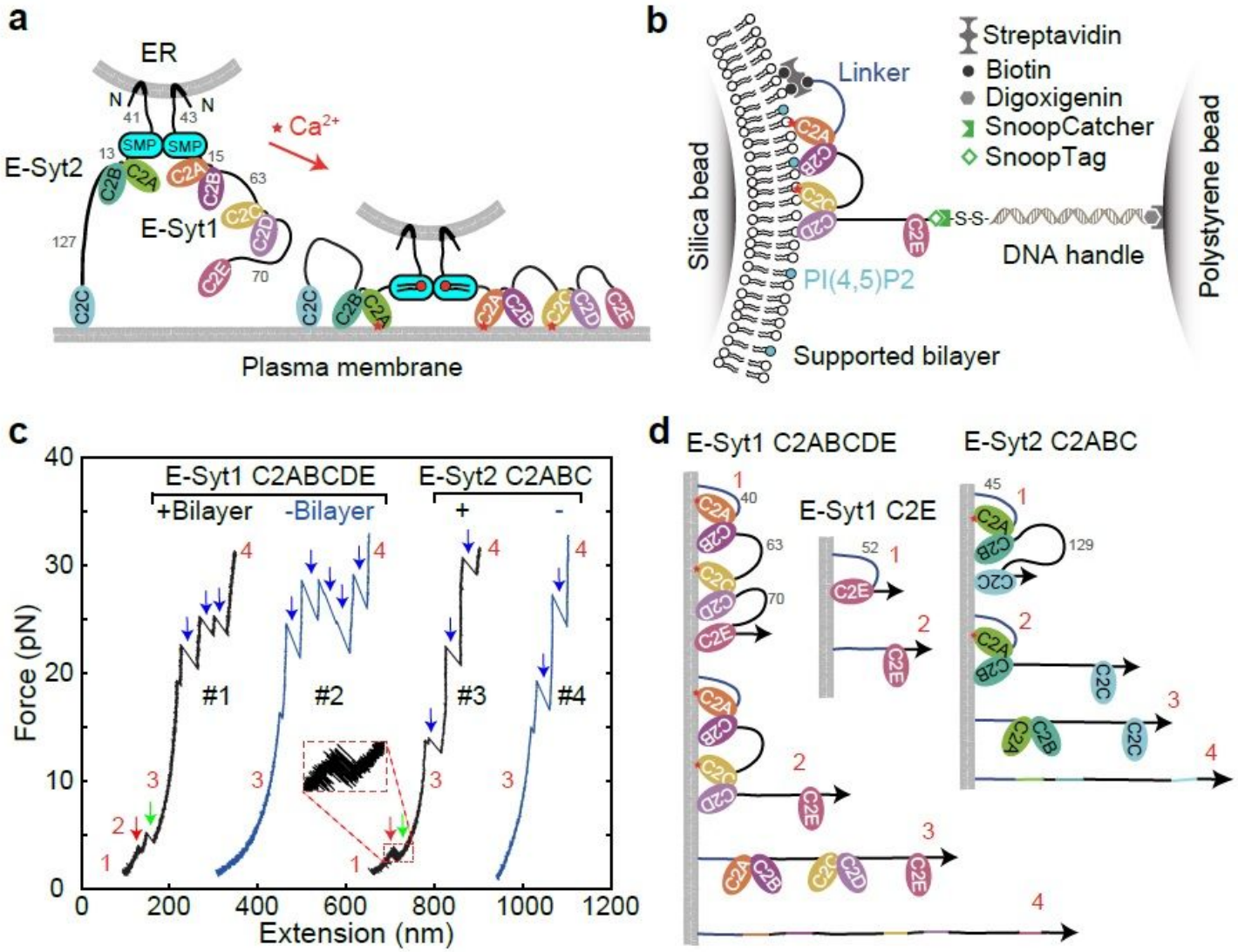

Figure 1

E-Syt C2 domains bind membranes in a stepwise manner as revealed by optical tweezers. (a) ER-anchored E-Syts form a dimer via their SMP domains and bind to the plasma membrane (PM) via their tandem C2 domains, pulling the ER-PM membrane close to facilitate lipid transfer in a Ca2+-dependent manner. The lengths of disordered linkers joining different C2 domains are indicated by their numbers in amino acids. (b) Schematics of the experimental setup to pull a single E-Syt1 C2 repeat C2ABCDE. (c) Force-extension curves (FECs) obtained by pulling single C2 repeats in the presence or absence of the lipid bilayer. Red and green arrows indicate stepwise C2 unbinding from the membrane, and black arrows denotes unfolding of individual C2 domains. (c) Schematics of different C2 binding states for some C2 domains or repeats tested in this study.

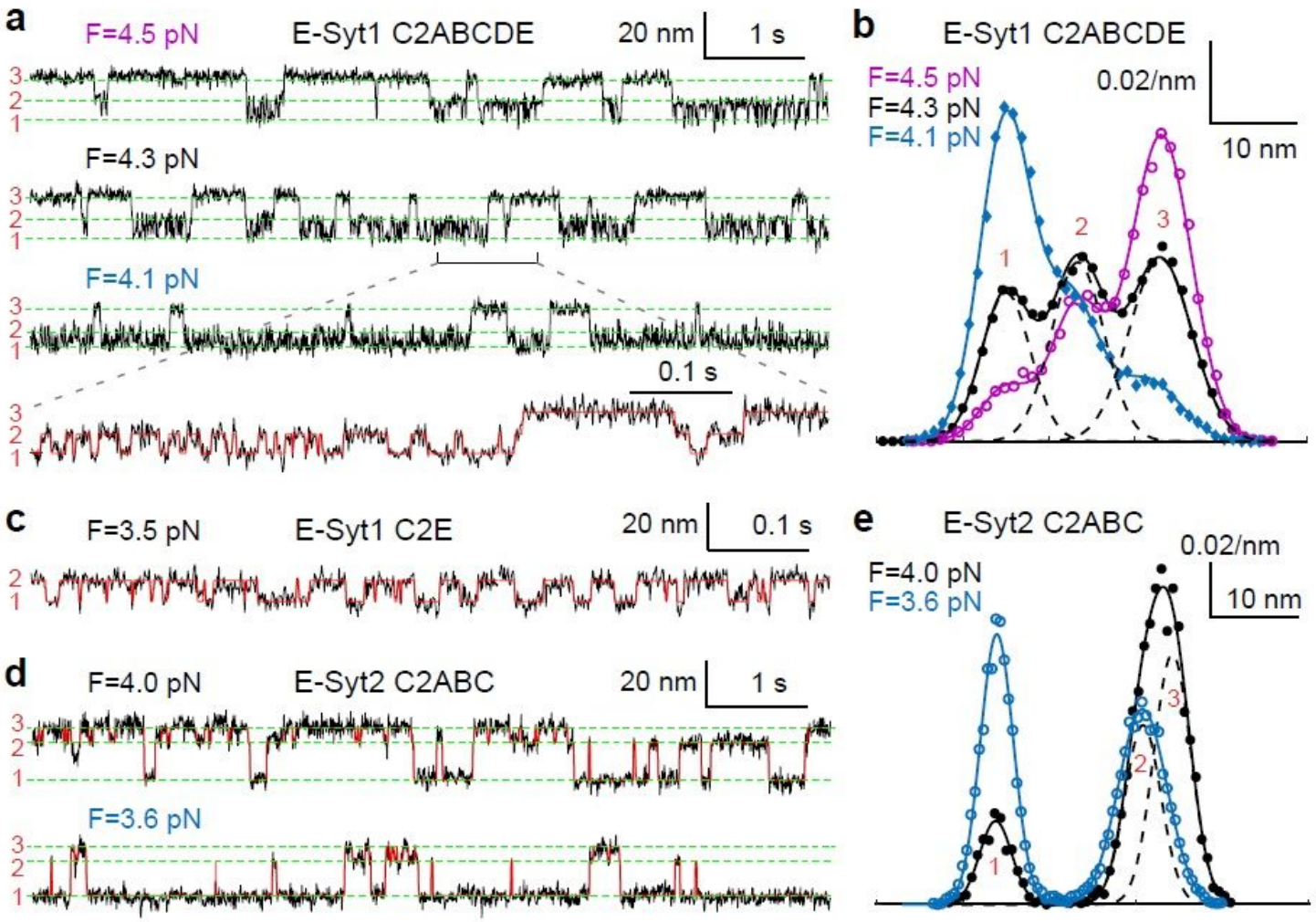

Figure 2

E-Syt C2 domains reversibly and sequentially bind to membranes. (a, c, d) Extension-time trajectories at constant mean force F for the C2 repeat E-Syt1 C2ABCDE (a), E-Syt1 C2C (c), or E-Syt2 C2ABC (d). The average extensions of three states (numbered on the left as in Fig. 1d) are marked by green dashed lines. A close-up view of the indicated region in the second trajectory in a is shown in the fourth trajectory. The overlaying red trace represents an idealized state transition derived from hidden-Markov modeling (HMM), as in other extension-time trajectories. (b, e) Probability density distributions of the extensions shown in a or d (symbols) and their best fits with a sum of three Gaussian functions (solid curves), with the individual Gaussian functions shown as dashed curves for the black curves.

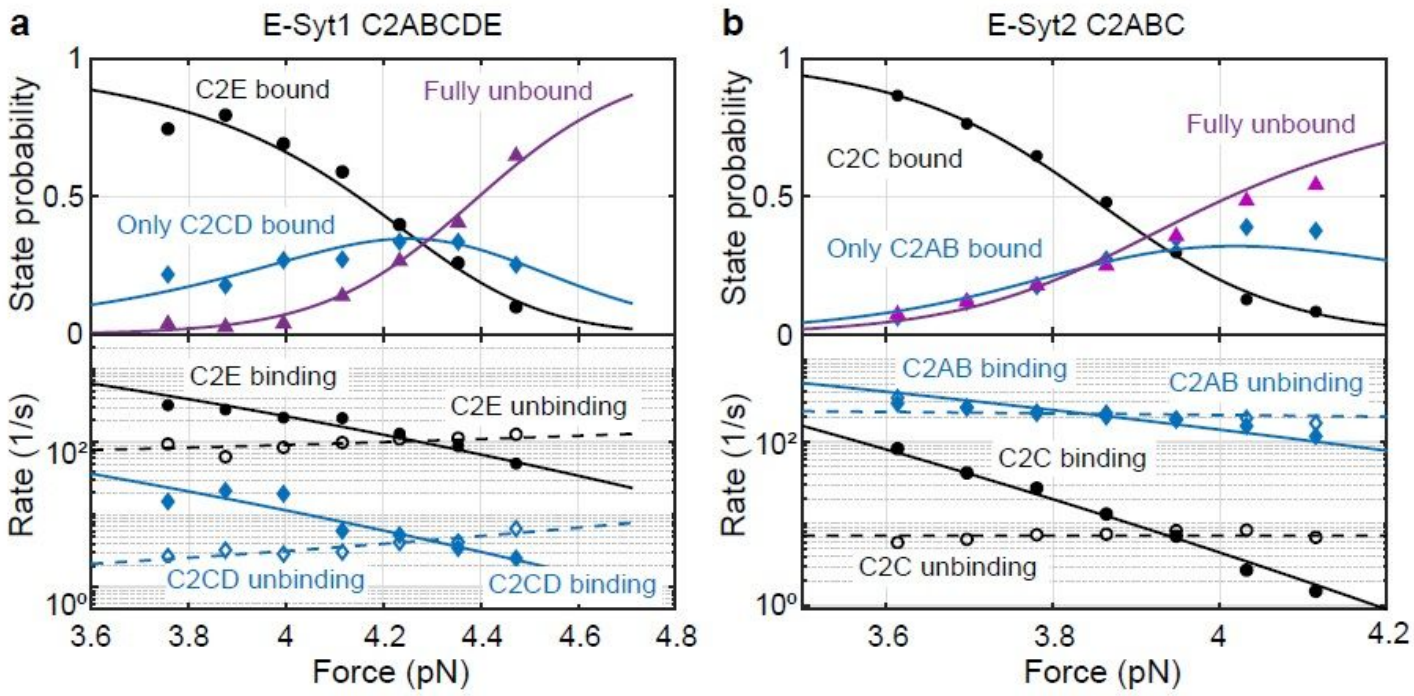

Figure 3

Force-dependent probabilities and transition rates of different C2 binding sates for E-Syt1 C2ABCDE (a) and E-Syt2 C2ABC (b). Experimental measurements and their best model fits (see Methods) are indicated by symbols and lines, respectively. The experiments were conducted with 85 mol% POPC, 10 mol% DOPS, 5 mol% PI(4,5)P2, and 0.03 mol% biotin-PEG-DSPE in the presence of 100 μM Ca2+.

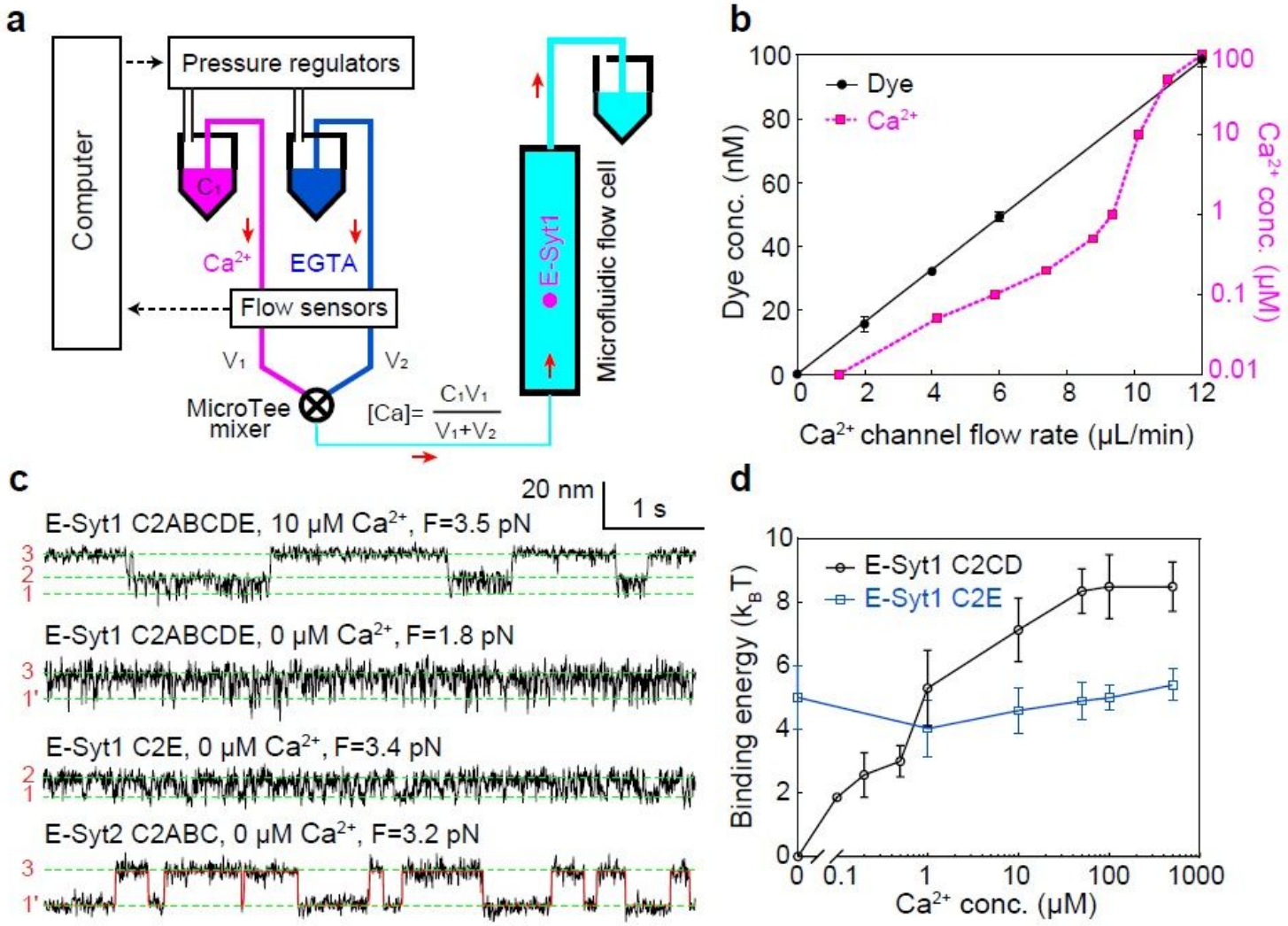

Figure 4

Membrane binding of E-Sty1 C2CD and E-Syt2 C2AB is Ca2+-dependent, while binding of E-Syt1 C2E and E-Syt2 C2C is Ca2+-independent. (a) Schematics of the microfluidic system to change Ca2+ concentration when a single C2 repeat was being pulled. (b) The measured tracing dye concentration and predicted free Ca2+ concentration in the flow cell as the flow rate of the Ca2+ channel linearly increased from 0 to 12 μL/min while keeping the total flow rate of the two channels at 12 μL/min. (c) Extension-time trajectories at constant force in different Ca2+ concentrations. (d) Unbinding free energy of E-Syt1 C2CD and C2E as a function [Ca2+].

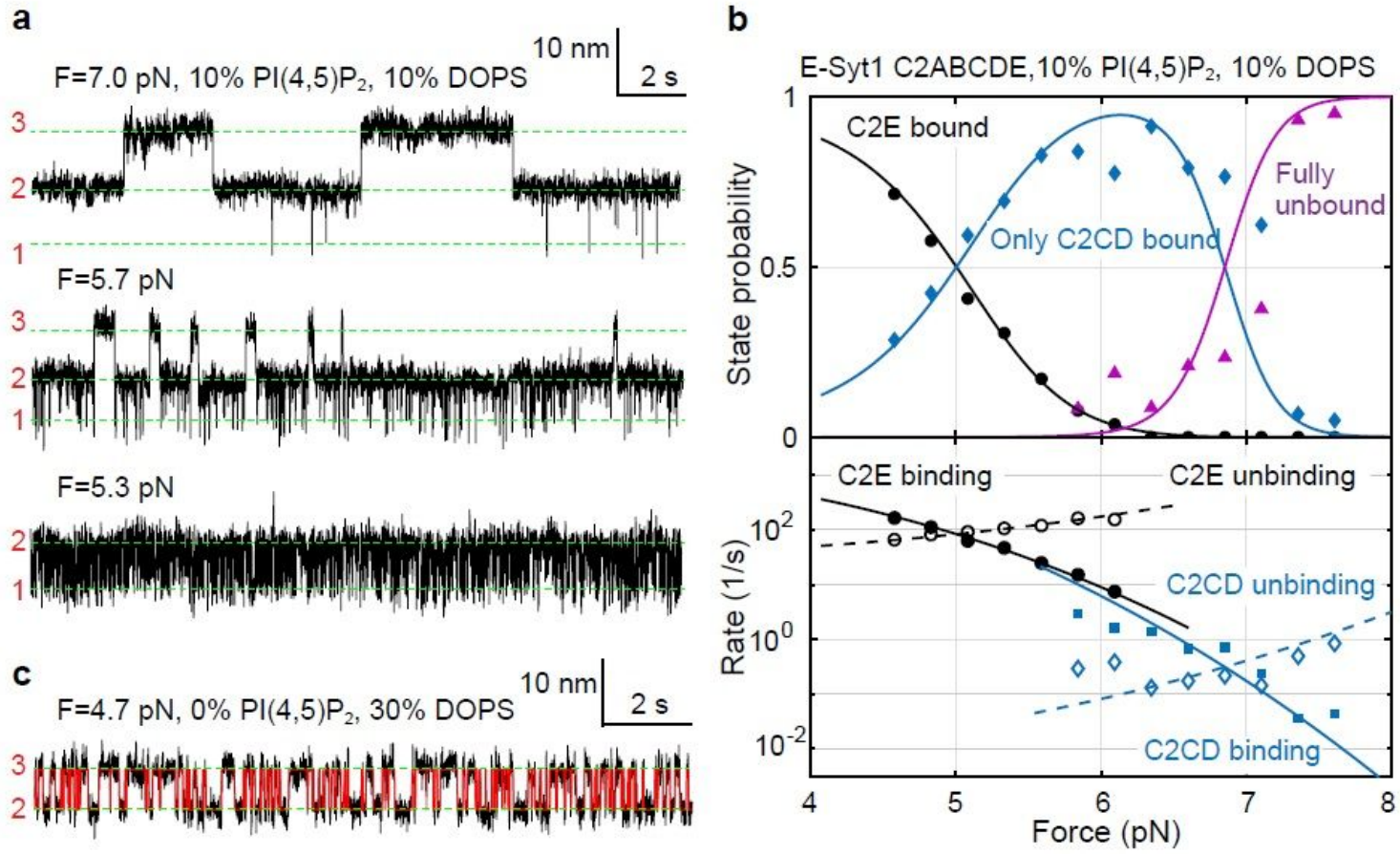

Figure 5

Membrane binding of E-Syt1 C2CD and C2E differentially depends upon PI(4,5)P2 and DOPS. (a) Extension-time trajectories of E-Syt1 C2ABCDE at constant force with 10 mol% PI(4,5)P2. (b) Force-dependent probabilities and transition rates of different E-Syt1 binding states (symbols) and their best model fits (lines). (c) Extension-time trajectory of E-Syt1 C2ABCDE at constant force in the presence of 30% DOPS.

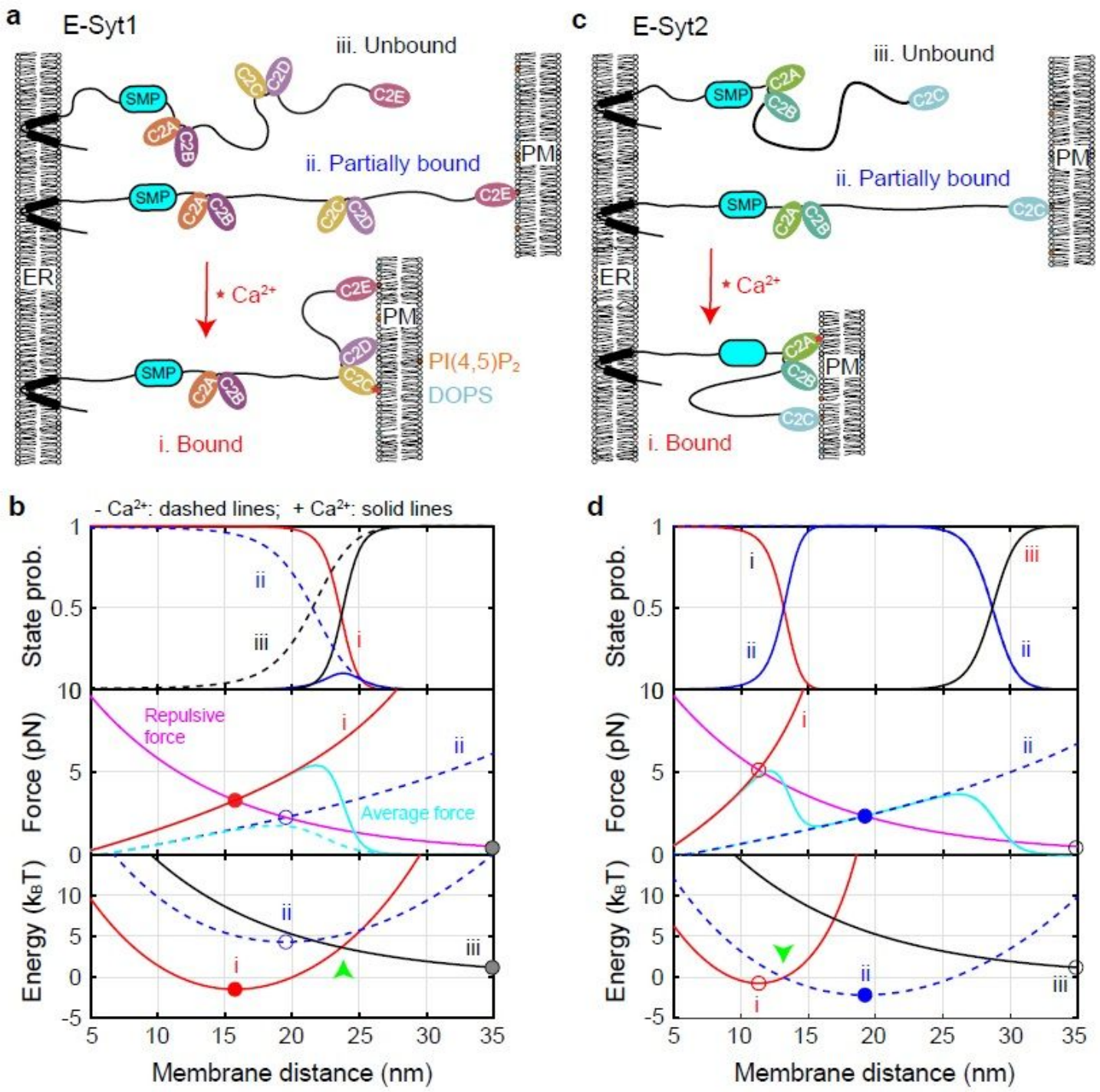

Figure 6

Properties of E-Syt-mediated ER-PM contacts can be theoretically modeled. (a, c) Schematics of different C2 binding and membrane tethering states of E-Syt1 (a) or E-Syt2 (c) in the absence and presence of Ca2+. (b, d) Calculated probabilities (top panel), tethering force (middle), and total free energy (bottom) of different states of E-Syt1 (b) or E-Syt2 (d). Calculations corresponding to the presence of Ca2+ or the absence of Ca2+ are indicated by solid and dashed lines, respectively. Stable and unstable states are indicated by solid and hollow circles, respectively.

Supplementary Files

This is a list of supplementary files associated with this preprint. Click to download.

- GeSupplementaryinformationMay12.docx
- SupplmentaryFigures.pdf